

Article

Dynamic Magnetic Fields Remote Control Apoptosis Via Nanoparticle Rotation

Enming Zhang, Moritz F Kircher, Martin Koch, Lena Eliasson, S. Nahum Goldberg, and Erik Renström

ACS Nano, Just Accepted Manuscript • DOI: 10.1021/nn406302j • Publication Date (Web): 05 Mar 2014

Downloaded from <http://pubs.acs.org> on March 8, 2014**Just Accepted**

“Just Accepted” manuscripts have been peer-reviewed and accepted for publication. They are posted online prior to technical editing, formatting for publication and author proofing. The American Chemical Society provides “Just Accepted” as a free service to the research community to expedite the dissemination of scientific material as soon as possible after acceptance. “Just Accepted” manuscripts appear in full in PDF format accompanied by an HTML abstract. “Just Accepted” manuscripts have been fully peer reviewed, but should not be considered the official version of record. They are accessible to all readers and citable by the Digital Object Identifier (DOI®). “Just Accepted” is an optional service offered to authors. Therefore, the “Just Accepted” Web site may not include all articles that will be published in the journal. After a manuscript is technically edited and formatted, it will be removed from the “Just Accepted” Web site and published as an ASAP article. Note that technical editing may introduce minor changes to the manuscript text and/or graphics which could affect content, and all legal disclaimers and ethical guidelines that apply to the journal pertain. ACS cannot be held responsible for errors or consequences arising from the use of information contained in these “Just Accepted” manuscripts.



1
2
3
4
5
6
7
8
9
10
11
12
13
14
15
16
17
18
19
20
21
22
23
24
25
26
27
28
29
30
31
32
33
34
35
36
37
38
39
40
41
42
43
44
45
46
47
48
49
50
51
52
53
54
55
56
57
58
59
60

Title

Dynamic Magnetic Fields Remote Control Apoptosis *Via* Nanoparticle Rotation

Authors

Enming Zhang^{1*#}, Moritz F. Kircher^{2-4#}, Martin Koch⁵, Lena Eliasson¹, S. Nahum Goldberg^{6, 7},
Erik Renström^{1*},

1) Department of Clinical Sciences Malmö, Lund University, Sweden;

2) Department of Radiology, Memorial Sloan-Kettering Cancer Center, New York, USA;

3) Department of Radiology, Weill Cornell Medical College, New York, NY, USA;

4) Center for Molecular Imaging and Nanotechnology, Memorial Sloan-Kettering Cancer Center,
New York, USA;

5) Stetter Elektronik, Seeheim-Jugenheim, Germany;

6) Laboratory for Minimally Invasive Tumor Therapies, Department of Radiology, Beth Israel
Deaconess Medical Center/Harvard Medical School, Boston, MA, USA;

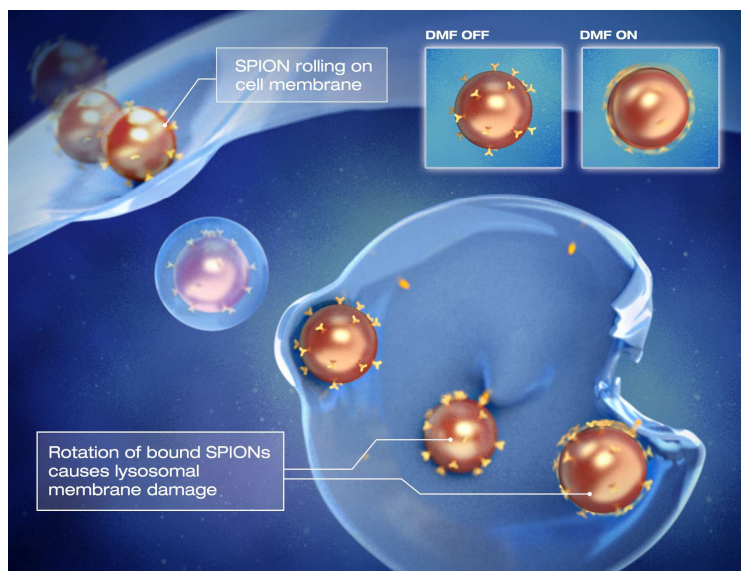
7) Division of Image-guided Therapy and Interventional Oncology, Department of Radiology,
Hadassah Hebrew University Medical Center, Jerusalem, Israel

*Address correspondence to Erik Renström, erik.renstrom@med.lu.se or Enming Zhang,
enming.zhang@med.lu.se.

#These authors contributed equally to this work

ABSTRACT

The ability to control the movement of nanoparticles remotely and with high precision would have far-reaching implications in many areas of nanotechnology. We have designed a unique dynamic magnetic field (DMF) generator that can induce rotational movements of



superparamagnetic iron oxide nanoparticles (SPIONs). We examined whether the rotational nanoparticle movement could be used for remote induction of cell death by injuring lysosomal membrane structures. We further hypothesized that the shear forces created by the generation of oscillatory torques (incomplete rotation) of SPIONs bound to lysosomal membranes would cause membrane permeabilization, lead to extravasation of lysosomal contents into the cytoplasm, and induce apoptosis. To this end, we covalently conjugated SPIONs with antibodies targeting the lysosomal protein marker LAMP1 (LAMP1-SPION). Remote activation of slow rotation of LAMP1-SPIONs significantly improved the efficacy of cellular internalization of the nanoparticles. LAMP1-SPIONs then preferentially accumulated along the membrane in lysosomes in both rat insulinoma tumor cells and human pancreatic beta-cells due to binding of LAMP1-SPIONs to endogenous LAMP1. Further activation of torques by the LAMP1-SPIONs bound to lysosomes resulted in rapid decrease in size and number of lysosomes, attributable to tearing of the lysosomal membrane by the shear force of the rotationally activated LAMP1-SPIONs. This remote activation resulted in an increased expression of early and late apoptotic

1
2
3 markers and impaired cell growth. Our findings suggest that DMF treatment of lysosome-
4
5 targeted nanoparticles offers a non-invasive tool to induce apoptosis remotely and could serve as
6
7 an important platform technology for a wide range of biomedical applications.
8
9

10 11 12 **KEY WORDS**

13
14
15 Dynamic magnetic field; nanoparticle rotation; iron oxide; magnetic nanoparticles; lysosomes;
16
17 antibody; LAMP1; permeabilization; apoptosis.
18
19
20
21
22
23
24
25
26
27
28
29
30
31
32
33
34
35
36
37
38
39
40
41
42
43
44
45
46
47
48
49
50
51
52
53
54
55
56
57
58
59
60

1
2
3 Superparamagnetic iron oxide nanoparticles have found wide-spread applications in the
4 biomedical field spanning *in vitro* diagnostic tests such as nanosensors,¹⁻⁴ *in vivo* imaging⁵⁻⁹ and
5 therapies such as magnetic fluid hyperthermia^{10,11} or drug delivery.^{12,13} Recent investigations
6 have also explored the capability of controlling the position or temperature of magnetic
7 nanoparticles within cells and tissues by remote application of magnetic fields. So far, this has
8 been investigated using permanent magnets that set nanoparticles in a longitudinal motion, using
9 alternating magnetic fields, or through rotating permanent magnets outside of the tissues of
10 interest.^{14,15} In the latter scenario, the nanoparticles describe circular motions, but do not
11 individually rotate around their own axis. The combination of alternating magnetic fields and
12 magnetic nanoparticles allows one to transform energy into forces or heat.^{16,17} Hyperthermia is
13 used as an adjunctive treatment in cancer therapy; here, high-frequency alternating (but not
14 moving) magnetic fields in the KHz/MHz range have been used to kill cancer cells loaded with
15 magnetic nanoparticles through thermal induction.¹⁸⁻²⁰ However, such treatment is not without
16 risks particularly near thermally sensitive structures such as the gut or gallbladder if
17 nanoparticles are injected systemically, as the heat induction cannot be controlled spatially with
18 high precision and could cause tissue necrosis. Therefore, in contrast to thermal ablation systems
19 ambient temperature increases $> 46^{\circ}\text{C}$ are not desirable for purposes of remote controlling
20 apoptosis with magnetic fields.²¹

21
22 Fundamentally different from prior studies using high frequency alternating magnetic fields that
23 cause apoptosis *via* heat induction, we describe here a principle of controlling nanoparticle
24 rotation and inducing apoptosis *via* mechanical forces exerted on membranes by targeted
25 nanoparticles. Specifically, we have developed a device that enables to induce and precisely
26 control the rotation of magnetic nanoparticles around their own axis, termed here ‘dynamic
27
28
29
30
31
32
33
34
35
36
37
38
39
40
41
42
43
44
45
46
47
48
49
50
51
52
53
54
55
56
57
58
59
60

1
2
3 magnetic field (DMF) generator'. The DMF generator creates a dynamic force field, which is
4
5 converted inside the particle into a magnetic flux field B , which operates on a SPION particle
6
7
8 with a magnetic Moment M and a moment of inertia I . The field generates a torque $\vec{\tau}$ equal
9
10 to $\vec{\tau} = \vec{\mu} \times \vec{B}$. This enables for the first time to induce rotation of individual magnetic nanoparticles
11
12 around their own axis, and allows precise control of the rotation speed.

13
14 We demonstrate that induction of this kind of rotation in targeted superparamagnetic iron oxide
15
16 nanoparticles (SPIONs) can be used to remotely activate apoptosis. We show that SPIONs
17
18 conjugated with LAMP1 (Lysosomal-associated membrane protein 1) antibodies (LAMP1-
19
20 SPION)²² internalize into cells and bind to lysosomal membranes. We observed that subsequent
21
22 remote activation of the dynamic magnetic field causes mechanical disruption of lysosomes,
23
24 which leads to apoptosis *via* extravasation of lysosomal contents into the cytoplasm and a
25
26 decrease of intracellular pH. While the unique ability of rotational control of nanoparticles is
27
28 demonstrated here in a specific biological application, the same principle should enable many
29
30 other new applications in the fields of nanotechnology and nanomedicine.
31
32
33
34
35
36
37
38
39
40
41
42
43
44
45
46
47
48
49
50
51
52
53
54
55
56
57
58
59
60

RESULTS

Dynamic magnetic field stimulation results in rotation of individual nanoparticles

A DMF generator was developed to control directional movement and self-centered rolling (**Fig. 1A**). To demonstrate the pattern of the particle movement, we first monitored the rotation of larger magnetic beads of different sizes (5.8, 1, 0.5 and 0.3 μm diameter) by filming them in a cell culture dish under a microscope. Once the DMF is switched on, the beads start to rotate around their own axis, which also causes a slow directional movement of the beads across the floor of the dish (**Fig. 2** and **web-Movie 1 & 2**). This clearly demonstrated that the applied DMF treatment enables a self-turning of magnetic particles. The speed of rotation can be controlled by varying the frequency setting on the DMF device (illustrated in **web-Movie 1 & 2**). This observation suggested that the DMF could be used to contrive a virus-like interaction between the SPIONs and the cell surface, which in turn could enhance internalization of the SPIONs into the cytosol. Once the SPIONs have internalized into the intracellular compartments, *e.g.* endosomes or lysosomes, the loaded SPIONs can be operated non-invasively by DMF to regulate the cellular compartmental activities and further cell functions (**Fig. 1B**).

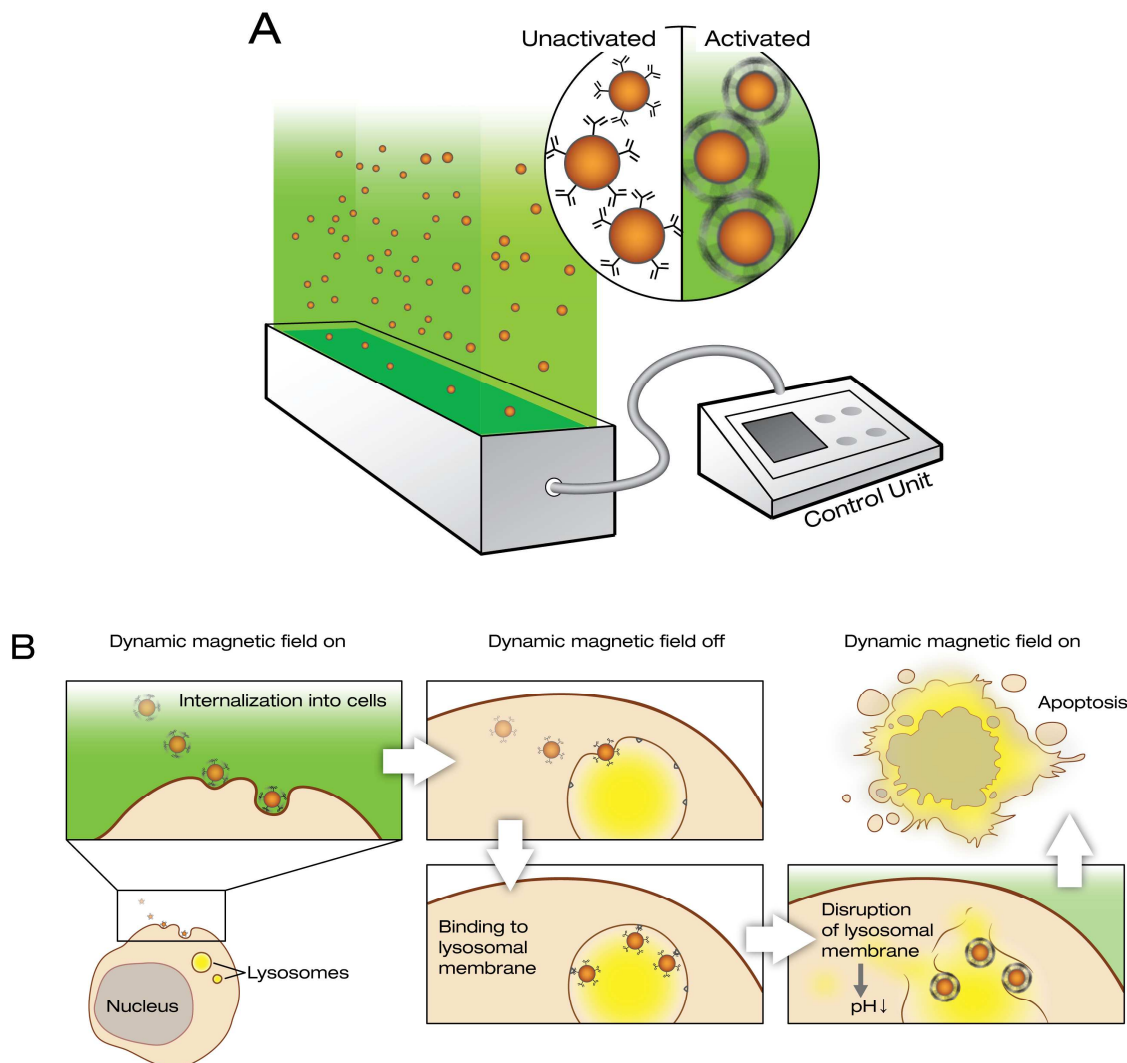


Figure 1. DMF controls rotation of magnetic nanoparticles.

(A) Schematic representation of the DMF generator. The device controls rotation and movement of magnetic nanoparticles (SPIONs) with a low frequency (10-40Hz) field. In contrast to reported alternating magnetic field generators, the DMF generator causes the nanoparticles to rotate around their own axis.

(B) Principle of use of the DMF generator: Remote induction of apoptosis. When targeted nanoparticles (LAMP1-SPIONs) first come into contact with cell membranes, their internalization can be enhanced by activation of slow nanoparticle rotation. This causes rotational motion (rolling) of the nanoparticles across the cell membrane and eventually internalization. Once internalized, the LAMP1-SPIONs enter lysosomes and bind to the lysosomal membrane. When the DMF is activated at this point, the nanoparticles start to rotate and the resulting shear forces cause injury to the lysosomal membrane. This in turn causes leakage of the lysosomal contents into the cytoplasm, leading to a decrease in its pH and subsequently apoptosis.

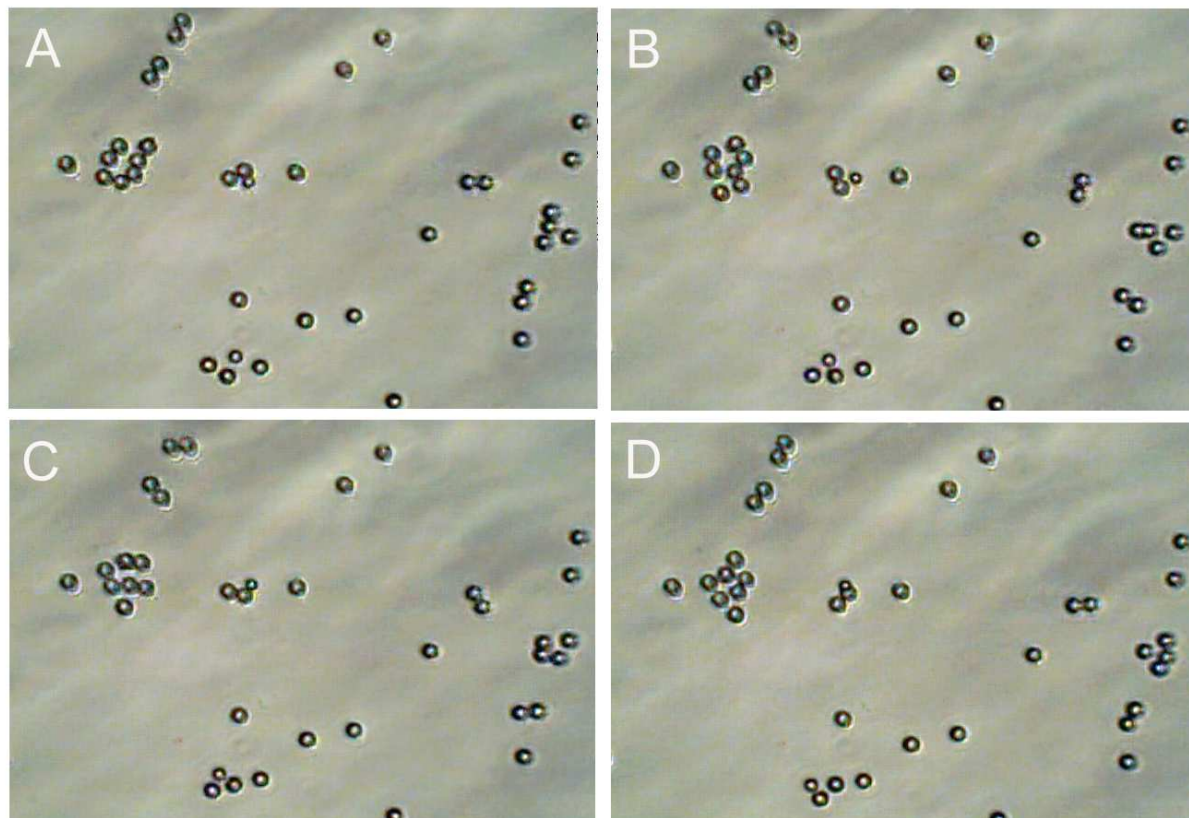
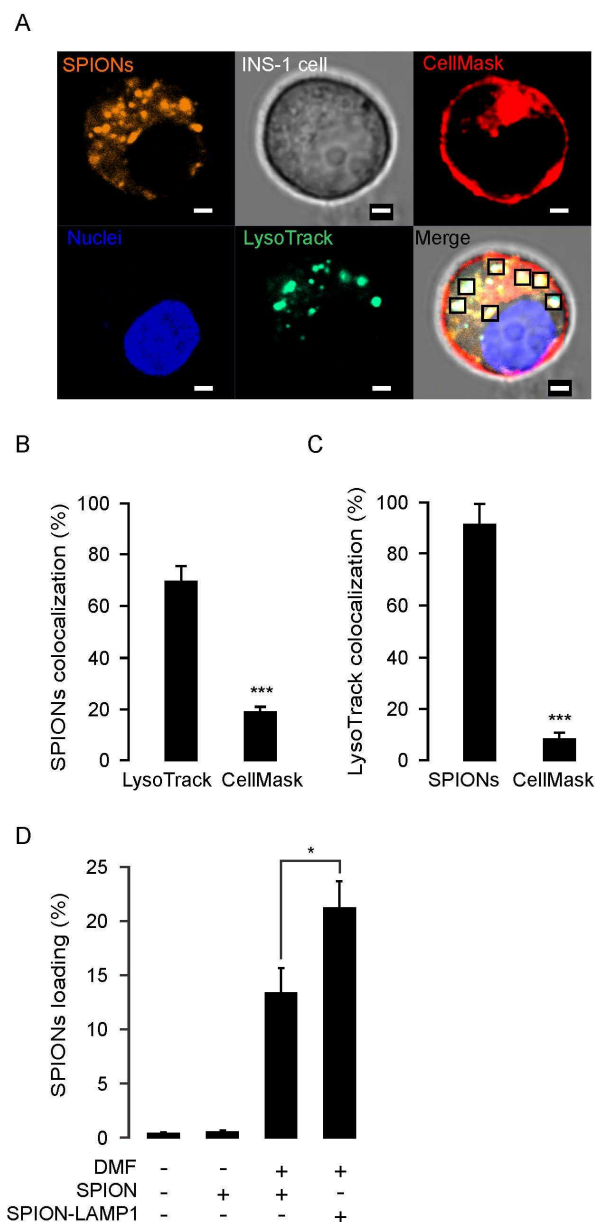


Figure 2. Illustration of DMF-induced rotation of magnetic particles. In order to enable better visualization of the effect of the DMF on magnetic particles under the microscope, larger micrometer sized magnetic beads (diameter 5.8 μm) were used. A dish containing beads in a physiologic salt solution (Krebs buffer) was placed in the vicinity of the DMF device. Once the DMF is switched on, the beads start to rotate around their own axis, which also causes a slow directional movement of the beads across the floor of the dish. The beads complete a rotation of 360° in seconds (time depends on the viscosity of the liquid) between the images A and D. The speed of rotation can be controlled by varying the frequency setting on the DMF device and in this experiment was varied between 5-15 Hz. This can be better appreciated in the accompanying **web-Movie 1**.

Dynamic magnetic field stimulation enhances uptake of superparamagnetic nanoparticles

1
2
3
4
5
6
7 Internalization of SPIONs into living cells was reported previously.²³⁻²⁵ We first evaluated the
8
9 internalization efficiency in the absence or presence of DMF stimulation. To monitor the process
10
11 of SPION internalization, we used fluorescently labeled (TRITC) 100-nm SPIONs and incubated
12
13 them with rat insulinoma cells (INS-1). We also tested 300-nm SPIONs, but these exhibited
14
15 markedly lower loading efficiency. We then applied a DMF field for 20 min. at a frequency of
16
17 20 Hz, before staining the cells using the plasma membrane marker CellMask, the lysosomal
18
19 marker LysoTracker Green and the nuclear marker Hoechst 34580. The cells were then imaged
20
21 by live confocal microscopy, which demonstrated that the majority of the SPIONs were loaded
22
23 into the lysosomes after 20 min. of DMF treatment (**Fig. 3A**). 71.2±3.8% of SPIONs colocalized
24
25 with the lysosomal marker LysoTracker Green, while only 18.2±2.2% of SPIONs colocalized
26
27 with the plasma membrane and early endosome probe CellMask (**Fig. 3B**). Conversely, 91±8.7%
28
29 of the LysoTracker Green fluorescence appeared in conjunction with SPIONs, which means that
30
31 nearly all lysosomes contained several loaded SPIONs (**Fig. 3C**). Next we conjugated SPIONs
32
33 with an antibody against the lysosomal membrane protein, LAMP1 (LAMP1-SPION). We
34
35 compared the loading efficiencies between SPION and LAMP1-SPION, in order to evaluate if
36
37 the conjugation of the LAMP1 antibody enhanced internalization and loading into the lysosomes.
38
39 LAMP1-SPION nanoparticles were more efficiently loaded into the lysosomes than the
40
41 unconjugated SPIONs, and the loading efficiency after 20 min. DMF treatment averaged
42
43 13.3±2.3% and 21.2±2.4% for SPIONs and LAMP1-SPIONs, respectively (**Fig. 3D**).
44
45
46
47
48
49
50
51
52
53
54
55
56
57
58
59
60

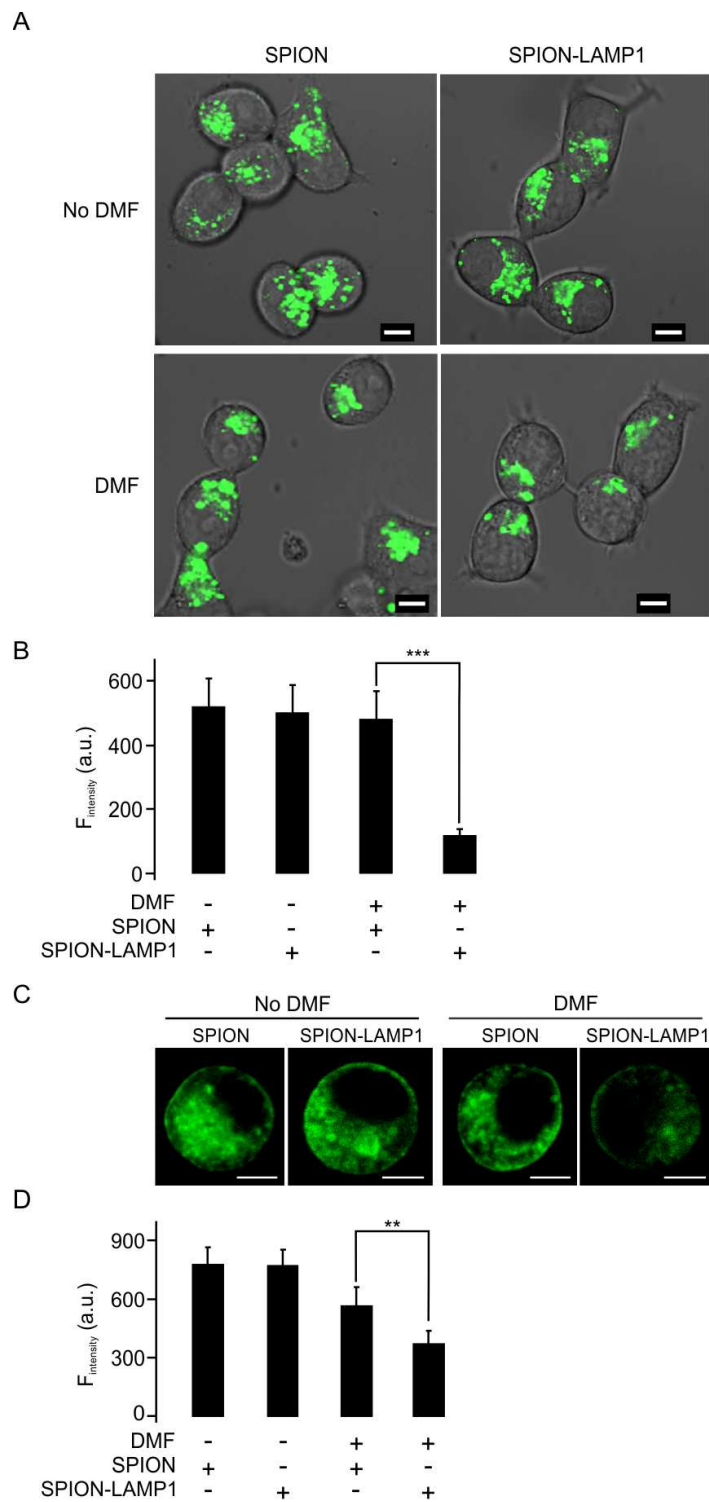


42 **Figure 3. Loading of magnetic nanoparticle into lysosomes in INS-1 cells.** (A) Confocal
43 imaging of SPIONs location in INS-1 cells. The SPIONs conjugated with the fluorescent dye
44 TRITC (orange) were incubated with living cells in a static magnetic field for 5 minutes.
45 Thereafter the cells were treated by DMF with 20 Hz, for 20 min. and then confocal microscopy
46 images obtained. Plasma membrane and early endosomes were stained with CellMask (red);
47 nuclei and lysosomes were stained with Hoechst 32580 (blue) and LysoTracker Green (green),
48 respectively. The squares in the merge stack indicate SPIONs located in the lysosomes. Scale
49 bars = 2 μ m. (B) Statistical analysis of SPION co-localization with LysoTracker Green and
50 CellMask under same conditions as in (A). (C) Co-localization analysis of lysosomes with
51 SPION and CellMask under same conditions as (A). (D) Loading efficiency of LAMP1 antibody
52 conjugated SPIONs (LAMP1-SPION) increased under condition with the DMF treatment. The
53 loading efficiency is calculated by the ratio of TRITC fluorescence intensity (yellow) over
54 nuclear intensity. The data was collected from three independent experiments. * $p < 0.05$ and ***
55 $p < 0.001$.
56
57
58
59
60

1
2
3 *Dynamic magnetic field stimulation can injure lysosomes via antibody-conjugated*
4 *superparamagnetic nanoparticles*
5
6
7
8
9

10 To evaluate whether DMF treatment has the potential to injure lysosomes in LAMP1-SPION-
11 loaded cells we visualized the lysosome compartment with the marker LysoTracker Green. After
12 DMF-facilitated loading of the LAMP1-SPION nanoparticles, the cells were cultured at 37 °C
13 for 40 min to allow binding of the antibody paratope on the nanoparticles to LAMP1 in the
14 lysosomal membrane. After that culture period, any remaining LAMP1-SPION nanoparticles
15 outside the cells were removed by washing, before subjecting the cells to DMF treatment (20 Hz)
16 for 20 minutes. The capability of the DMF treatment to disrupt the compartments of the
17 lysosomes was evaluated by assessing changes in LysoTracker Green fluorescence intensity.
18 Indeed, in LAMP1-SPION-loaded cells, the DMF treatment significantly decreased LysoTracker
19 Green fluorescence by 75% as compared to cells loaded with conventional SPIONs without the
20 LAMP1 antibody (483.6±84.2 A.U. vs. 120.3±20.9 A.U. for SPION- and LAMP1-SPION-
21 treated cells, respectively (**Fig. 4A** and **4B**). A dynamic depiction of this finding is shown in
22 **web-Movie 3** (green = LysoTracker Green; red = LAMP1-SPIONs). To confirm these findings,
23 we next used the acidotropic probe (pKa=5.2) LysoSensor Green DND 189.²⁶ The rationale for
24 this experiment was that disruption of lysosomes would reduce the volume of the very acidic
25 compartments in the cell and lead to a decrease in LysoSensor Green fluorescence (**Fig. 4C** and
26 **4D**). Prior to DMF treatment, we found no difference in fluorescence intensity between SPION-
27 and LAMP1-SPION-loaded cells. DMF treatment had no effect in SPION-loaded cells. In
28 contrast, in LAMP1-SPION-treated cells fluorescence intensity dropped (769.5±82.5 A.U./cell vs.
29
30
31
32
33
34
35
36
37
38
39
40
41
42
43
44
45
46
47
48
49
50
51
52
53
54
55
56
57
58
59
60

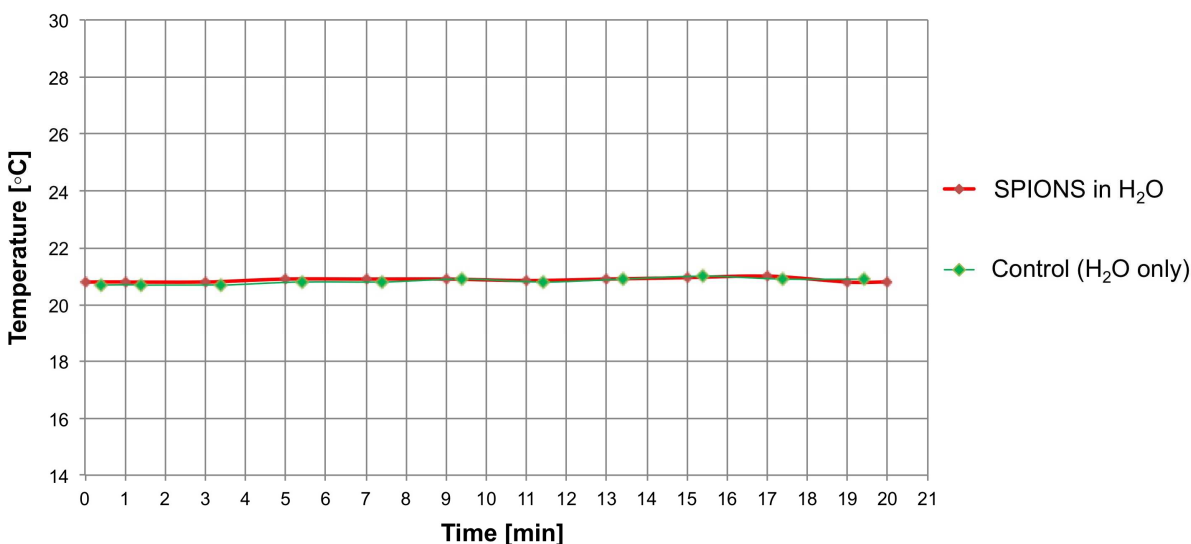
368.4±69.6 A.U./cell in SPION- vs. LAMP1-SPION treated cells, respectively; $P < 0.001$). While



the induction of heat – in contrast to

1
2
3 **Figure 4. DMF treatment decreases intracellular lysosomes and the pH in LAMP1-SPION**
4 **loaded INS-1 cells. (A)** The cells were treated by DMF (20 Hz, 20 min.) and lysosomes stained
5 with LysoTracker Green. Scale bars = 5 μm . **(B)** Mean intensity of fluorescence was measured
6 under the different conditions in (A). **(C)** Representative confocal images indicate the
7 intracellular pH value using an acidotropic probe, LysoSensor Green DND 189 in INS-1 cells.
8 Scale bars = 5 μm . **(D)** Mean fluorescence intensities were measured as in (C). Data collected
9 from five experiments with at least 6 cells under each condition. ** $p < 0.01$, *** $p < 0.001$.

10
11 high frequency alternating magnetic fields - was not expected a priori given the low frequency of
12
13
14 our dynamic magnetic fields, we excluded this possibility by monitoring temperature runs in
15
16 phantoms. These experiments showed that no significant change in temperature was caused by
17
18 the DMF induced magnetic field (**Fig. 5**). Taken together, these results suggest that the remote
19
20 application of the DMF treatment causes permeabilization of lysosomal compartments, induced
21
22 *via* the torque of the membrane-bound LAMP1-SPIONs.
23
24
25
26
27



46 **Figure 5. DMF-field induced SPION rotation does not increase temperature.** A dish with
47 100 nm SPIONs (10 mg/ml) in water and a control dish containing water only, each containing a
48 temperature probe, were placed simultaneously on the DMF device. The dishes were then
49 subjected to the DMF field for 20 min. at 20 Hz. No significant change in temperature was
50 observed in either the dish with the SPIONs (red curve) or the control dish (green curve).
51
52
53
54
55
56
57
58
59
60

1
2
3 *Effects of dynamic magnetic field stimulation of superparamagnetic nanoparticles in human*
4 *primary cells*
5
6
7

8
9
10 To monitor the LAMP1-SPION loaded lysosomes, we coated SPIONs covalently with both
11 LAMP1 antibodies and the fluorescence marker TRITC (TRITC-LAMP1-SPION). To further
12 validate the possibility to translate our findings to clinical settings, we used isolated primary cells
13 from human pancreatic islets and seeded on glass bottom petri dishes. Then TRITC-LAMP1-
14 SPIONs were added to cell culture medium, followed by DMF treatment or no treatment, and
15 finally the cells were fixed for confocal microscopy. Human primary islet cells contained larger
16 lysosomes than INS-1 cells as assessed by TRITC fluorescence (**Fig. 6A**, upper). To assess co-
17 localization of LAMP1 and TRITC-LAMP1-SPION, LAMP1 was detected by indirect
18 immunocytochemistry using a Cy2-tagged secondary antibody. In cells not exposed to DMF
19 treatment, LAMP1 and TRITC-LAMP1-SPION co-localized by $49.9\pm 9.2\%$, which was not
20 significantly affected by DMF treatment ($54.8\pm 9.5\%$) (Data not shown). These results indicate
21 that the bonds between LAMP1 and TRITC remain stable during DMF treatment. Interestingly,
22 the TRITC-LAMP1-SPIONs loaded into the cells mainly appeared around the boundaries of
23 structures, which are likely to represent a location in the lysosomal membrane (**Fig. 6B**).
24 However, after a second round of DMF treatment most of the LAMP1 was apparently separated
25 from the TRITC-LAMP1-SPIONs (**Fig. 6A**, bottom) and the SPIONs aggregated tightly (**Fig.**
26 **6C**). DMF treatment also led to a marked downward shift in the distribution of lysosomal sizes
27 (**Fig. 6D**), and accordingly the average size of lysosomes decreased from $1.77\pm 0.06\ \mu\text{m}$ (n=141)
28 to $0.79\pm 0.05\ \mu\text{m}$ (n=105) after DMF treatment (**Fig. 6E**). These results suggest that the second
29 round of DMF treatment in cells loaded with TRITC-LAMP1-SPIONs results in a certain degree
30
31
32
33
34
35
36
37
38
39
40
41
42
43
44
45
46
47
48
49
50
51
52
53
54
55
56
57
58
59
60

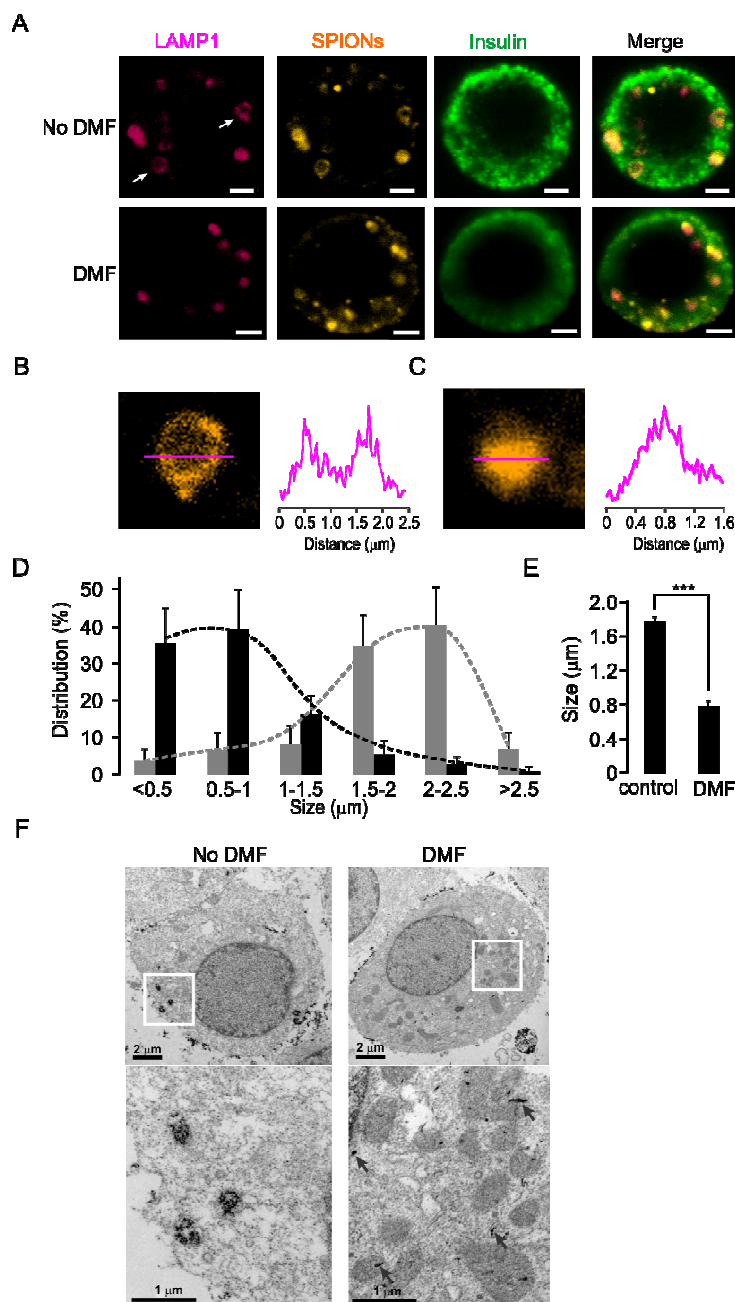


Figure 6. DMF treatment disrupts lysosomes in human pancreatic beta cells after loading with LAMP1-SPIONs. (A) Immunostaining of human islet beta cells with or without DMF treatment. Lysosomes were stained with the anti-LAMP1 antibody (red), SPIONs with TRITC (orange) and islet beta-cells with an anti-insulin antibody (green), respectively. Scale bars = 2 μm . (B) The SPIONs are located in the membrane of a lysosome. The intensity profile (right) was derived along the red line in the image (left). (C) Same as (B), except after treatment with DMF. (D) Differences in size distribution of lysosomes before (grey bars) and after (black bars) DMF treatment. (E) Average size of lysosomes without and with DMF treatment. *** $p < 0.001$. (F) Transmission electron microscopy (TEM) images of the intracellular distribution of SPIONs in INS-1 cells. Images on the bottom are magnified versions of the areas indicated with white boxes. While without DMF treatment the LAMP1-SPIONs are clustered in vesicular structures, their distribution is scattered throughout the cytosol after DMF treatment.

1
2
3 of damage to the lysosome membrane. However, a potential alternative explanation could be that
4 the detachment of TRITC-LAMP1-SPIONs occurs from the lysosome membrane without
5 disruption which can lead to the particles aggregating in the center of the still intact lysosomes.
6
7 To address this possibility, the subcellular locations of the LAMP1-SPIONs were further
8 identified by transmission electrical microscopy (TEM). The TEM images clearly showed that
9 LAMP1-SPION particles had accumulated within intracellular compartments after loading into
10 cells (**Fig. 6F**, left). In contrast, after the second round of DMF treatment, the LAMP1-SPIONs
11 were scattered throughout the cells (**Fig. 6F**, right). These results demonstrate that DMF-induced
12 rotational movement of LAMP1-SPIONs are also capable of disrupting lysosomal membranes in
13 human primary cells.
14
15
16
17
18
19
20
21
22
23
24
25
26
27
28

29 *Consequences of DMF-mediated disruption of lysosomes*

30
31
32
33

34 Disruption of lysosomes has previously been reported to activate apoptotic reactions.²⁷ To
35 determine whether DMF treatment can elicit apoptosis in LAMP1-SPION-loaded cells, we
36 measured the extent of apoptosis in INS-1 cells with and without DMF. Annexin V and 7-AAD
37 were used to indicate early and late stage apoptosis, respectively (**Fig. 7A**). After DMF treatment,
38 early and late apoptosis in LAMP1-SPION loaded INS-1 cells significantly increased from
39 4.56±0.55% to 12.45±1.6% and from 0.73±0.17% to 1.31±0.16%, as evidenced by positive
40 staining for Annexin V or 7-AAD, respectively (**Fig. 7B** and **7C**). Furthermore, the elevated rates
41 of apoptosis also had consequences on cell proliferation during culture. A single 20 min. DMF
42 treatment (20Hz) in SPION-loaded cells had no significant effect on cell number during a 6-days
43 culture period when compared to control cells. In contrast, the number of LAMP1-SPION loaded
44
45
46
47
48
49
50
51
52
53
54
55
56
57
58
59
60

cells after DMF treatment was significantly ($p < 0.001$) lower from day 2 and onwards (**Fig. 7D**). These results suggest that the attack on lysosomes *via* DMF-activated lysosomal membrane-targeted SPIONs prompts apoptotic cell death and affects the growth of the cell population.

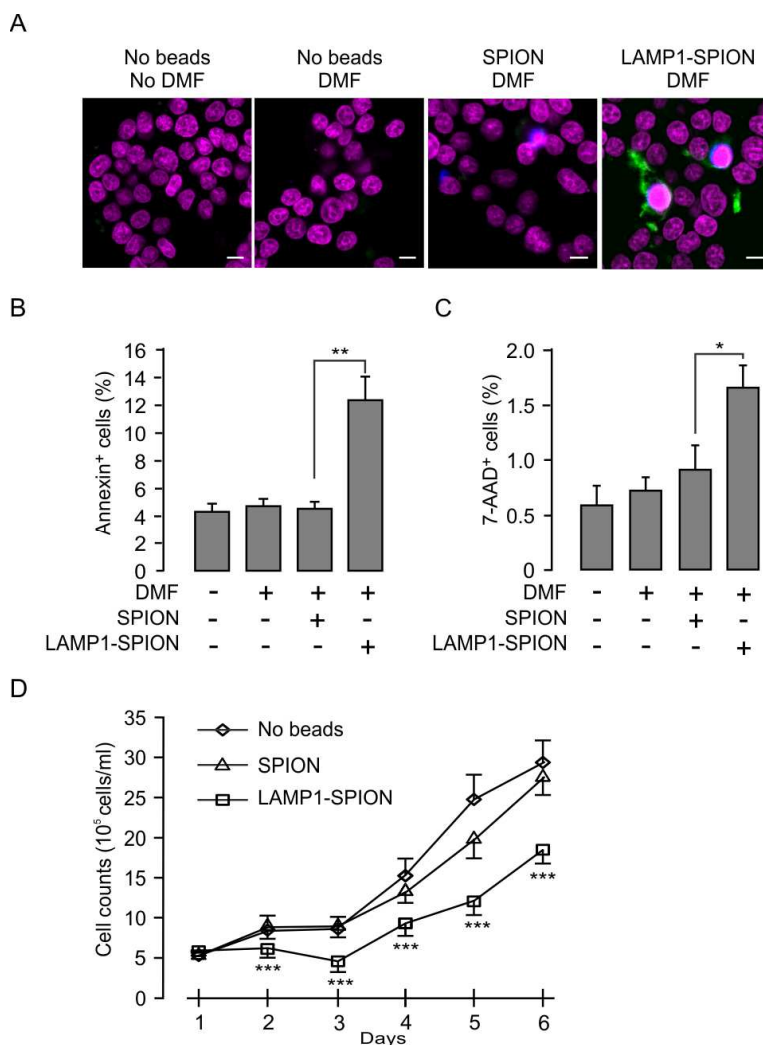


Figure 7. DMF treatment-induced apoptosis in LAMP1-SPION loaded cells. (A) The INS-1 cells were treated with DMF for 20 min. at 20 Hz and stained with the nuclear marker Hoechst (purple), the apoptosis marker annexin V (green) and 7-AAD (blue). Scale bars = 5 μm . After 6 hours of incubation (5% CO_2 , 37 $^\circ\text{C}$), early (B) and late (C) stage apoptosis was detected by percentage of number of annexin V and 7-AAD positive cells to the number of Hoechst stained cells. Note that DMF caused significant increase in apoptosis in LAMP1-SPION-loaded cells compared to when loading was done using conventional SPIONs. Each treatment was conducted with 28 cells. * $p < 0.05$. (D) Decrease of the rate of cell growth in LAMP1-SPION loaded INS-1 cells. Cells were treated with DMF (20Hz, 20 min.) once/day. Data are from 3 independent experiments and represent mean values \pm S.E.M.. *** $p < 0.001$.

DISCUSSION

Here we described a novel biomedical platform based on a unique dynamic magnetic field generator, which in combination with superparamagnetic nanoparticles can be utilized for various new applications.

Several prior studies have investigated the effect of ‘alternating magnetic fields’ on magnetic nanoparticles.^{14,15,18,28-31} These studies generally used high-frequency (kHz range) alternations in the magnetic field polarity, and observed that targeted iron oxide nanoparticles caused damage to cellular membranes leading to permeabilization. Energy dissipated locally as heat by the iron oxide nanoparticles was thought to lead to disruption of lipid bilayers. Huang *et al.*³² demonstrated a temperature-induced change in fluorescence when a fluorochrome was attached to a magnetic nanoparticle and exposed to an alternating magnetic field, whereas no change was observed in free fluorochromes.

In contrast to these reports using high-frequency alternating (but not dynamic) magnetic fields, our DMF approach uses low-frequency (~ 10-20 Hz), dynamic (*i.e.* moving) magnetic fields of ~30 mT that uniquely induce rotation of every individual particle in the field around their own axis (Fig. 1, web movie 1 and 2). The speed of this rotation (and its direction) can be controlled by varying the frequency setting on the device. For example, at lower frequencies nanoparticles can be prompted to roll over cell membranes, which may mimic the movement of viruses along cell membrane surfaces³³ and increase the efficiency with which nanoparticles internalize into cells. Higher rotational speeds can be used in order to destroy particular targets *via* rotational shear forces without inducing unwanted thermal effects. Molecular simulations of lipid bilayers have shown that both incremental shear and tension can destabilize cell membranes, and that the energy that is required to cause such membrane damage can be achieved with rotating magnetic

1
2
3 nanoparticles.^{15,34} We have applied the DMF on LAMP1 antibody-conjugated
4
5 superparamagnetic iron oxide nanoparticles to facilitate nanoparticle uptake into cells and to
6
7 disrupt the lysosomal membrane as a means to induce cell apoptosis. The DMF approach has two
8
9 major advantages: 1) Nanoparticles can be rotated around their own axis, and 2) No significant
10
11 heat is created. Heat creation is the presumed mechanism of how high-frequency alternating
12
13 magnetic fields cause damage to cell membranes.³¹ This however can potentially cause
14
15 extensive and unspecific cellular necrosis. By contrast, our DMF technology does not induce
16
17 heating above the physiological temperature range. By our method, apoptosis can be specifically
18
19 induced in nanoparticle-loaded cells only and apoptotic cells are removed *in vivo* by endogenous
20
21 scavenger systems *e.g.* the innate immune system and macrophages. Tissue damage is thus
22
23 limited to only the targeted cells, in contrast to procedures leading to supraphysiological
24
25 temperatures and resultant necrosis, potentially sparing wide-spread acute inflammatory
26
27 reactions.
28
29

30
31
32 To achieve a high degree of specificity of nanoparticle-mediated intervention, targeting of the
33
34 nanoparticles to the right cell type and into the desired subcellular compartment is important.
35
36 Our technology platform represents an example of unique utilization of DMFs to target magnetic
37
38 nanoparticles to specific intracellular compartments. Previous reports have demonstrated the
39
40 usefulness of magnetic nanoparticles for controlling activity of plasma membrane receptors or
41
42 ion channels.^{28,29,35} Upon protracted stimulation of receptors or ion channels there is solid
43
44 evidence for down-regulation of their activities. One important mechanism of such
45
46 desensitization is internalization of receptors or ion channels to intracellular sites where they
47
48 reside in an inactive standby pool. In the context of nanoparticle-mediated activation of receptors
49
50 or ion channels this means that after activation, the number of the receptors/ion channels in
51
52
53
54
55
56
57
58
59
60

1
2
3 plasma membrane decreases and the desired cellular signals and responses are blunted. Moreover,
4
5 the magnetic nanoparticles themselves are internalized already after short incubation with live
6
7 cells *via* the endocytotic pathway.^{36,37} We have made use of this property of internalization and
8
9 facilitated the process by DMF treatment to accelerate delivery of LAMP1 antibody-coated
10
11 nanoparticles to intracellular compartments. Following down the endocytotic pathway, the
12
13 LAMP1-SPIONs enter the early- and late-endosomes and afterwards they should enter other
14
15 compartments, *e.g.* ER, *via* recycling endosomes, or being removed from the lysosomes,³⁸ In the
16
17 lysosomes, the LAMP1 antibody conjugated to the SPION recognizes LAMP1 that is highly
18
19 expressed in the lysosomal membrane. In response to a low frequency DMF, the now bound
20
21 SPION generates dynamic forces strong enough to tear the lysosomal membrane, leading to
22
23 destruction of the lysosome integrity, leakage of lysosomal enzymes and finally induction of
24
25 apoptosis. In INS-1 cells, we observed that the SPIONs mostly loaded into lysosomes after 20
26
27 minutes DMF treatment (**Fig. 3A**). This preferential lysosomal localization was also observed
28
29 when SPIONs were located into primary human pancreatic islet cells (**Fig. 6A**). However, as the
30
31 direction and extent of intracellular membrane trafficking may differ markedly between cell
32
33 types, the lysosome loading efficiency needs to be carefully evaluated when adopting this
34
35 application to other cell types. Thus, we envisage that this technology will ultimately provide an
36
37 avenue for development of tools to regulate specific subcellular compartmental functions
38
39 including not only the nuclei, but also compartments such as the ER, Golgi apparatus and
40
41 different types of endosomes along the intracellular membrane trafficking system. Further
42
43 studies will be needed to translate our approach *in vivo*. Certain challenges such as the precise
44
45 delivery of the nanoparticles in a more complex *in vivo* scenario, and the application of DMF
46
47 fields in larger animals and humans in deep organs will have to be overcome. However, ultimate
48
49
50
51
52
53
54
55
56
57
58
59
60

1
2
3 clinical translation using our low frequency DMF approach may be more straightforward than
4
5 using high-frequency alternating fields, because the DMF fields are not expected to cause
6
7 nonspecific heating of tissues through induced eddy currents³¹ and should therefore have a better
8
9 safety profile.
10

11
12 The achievement of rotational control on nanoparticles with the DMF method has many other
13
14 potential applications beyond the model systems used here, in both biomedical and non-
15
16 biological nanotechnology fields. For example, magnetic actuation has been shown to control
17
18 timing and drug release from vesicles containing iron oxide nanoparticles.³⁹ The increase in
19
20 permeability of lysosomal membranes not only can be used to promote apoptosis, such as
21
22 through the release of proteolytic enzymes and increase in reactive oxygen species, but can also
23
24 increase the efficacy of drugs trapped in lysosomes. Because sequestration of drugs in lysosomes
25
26 is responsible for up to 40% of whole tissue drug uptake,⁴⁰ lysosomal drug trapping plays an
27
28 important role in the development of tumor drug resistance.⁴¹ Therefore, with further
29
30 development DMF-mediated lysosomal membrane permeabilization could be used to treat cancer
31
32 drug resistance.
33
34
35
36
37
38
39
40
41
42
43
44
45
46
47
48
49
50
51
52
53
54
55
56
57
58
59
60

CONCLUSIONS

In summary, using a unique dynamic magnetic field (DMF) generator we can control rotational movements of superparamagnetic iron oxide nanoparticles (SPIONs) in solution. This rotational nanoparticle movement was applied for remote induction of cell death by injuring lysosomal membrane structures. We covalently coated SPIONs with antibodies targeting the lysosomal protein marker LAMP1 (LAMP1-SPION). Remote activation of slow rotation of LAMP1-SPIONs with 20 Hz for 20min, significantly improved the efficacy of cellular internalization of the nanoparticles. $71.2\pm 3.8\%$ of LAMP1-SPIONs accumulated along the membrane in lysosomes in rat insulinoma tumor cells due to binding of LAMP1-SPIONs to endogenous LAMP1. Further activation of torques by the LAMP1-SPIONs bound to lysosomes resulted in rapid decrease in size and number of lysosomes, attributable to tearing of the lysosomal membrane by the shear force of the rotationally activated LAMP1-SPIONs. This remote activation resulted in increased cell apoptosis and impaired cell growth. Our findings suggest that DMF treatment of lysosome-targeted nanoparticles offers a non-invasive tool to induce apoptosis remotely and could serve as an important platform technology for a wide range of biomedical applications.

METHODS

Nanoparticle assembly. The protocol of conjugation of LAMP1 antibodies to magnetic nanoparticles was described previously.²² Briefly, SPION nanoparticles (Micromod, Germany) were amino-functionalized and the density of amino groups per mg of particles was determined. After washing, the other parts of amino groups were reacted with sulfo-SMCC in PBS-EDTA buffer to introduce maleimide groups on the particle surface. The monoclonal LAMP1 antibody (Abcam, UK) was purified with a G-25 column containing PBS/EDTA buffer to remove the glycerin and sodium azide. After purification the LAMP1 antibody was treated with imnothiolane solution to introduce the SH groups. After washing the SH-modified antibody with PBS-EDTA buffer in a G-25 column, the maleimide-modified particles were added. The particles were shaken for 1 h at room temperature. Then cystein was added to quench the remaining reactive sites. Finally the particles were purified with PBS buffer in magnetic columns in a high gradient magnetic field.

DMF device. The dynamic fields to control SPION rotation used in this study were created with a DMF generator (DM-01, Feldkraft and Stetter Elektronik, Germany). The device consists of an array of multiphase coil systems, where the coils are displaced against each other. The field can be altered in a highly dynamic fashion. A device-integrated digital controller regulates the frequency as well as the magnetic flux. The dynamic flux produces an electromagnetic gradient force $\vec{F} = (M\nabla) \cdot \vec{B}$, where \mathbf{M} are the magnetic moments of the beads in total and \mathbf{B} is the dynamic flux density field vector. This vector is established by the \mathbf{H} field of our device. The magnetic field strength generated by the DMF device used in this study is approx. as large as 30 mT (rms).

1
2
3 **Live cell imaging.** Cells were seeded onto glass coverslips. After DMF treatment, live images
4 were acquired using a Zeiss 510 Meta confocal system with a $\times 40$ water immersion objective
5 (NA=1.2). SPION-TRITC was visualized by excitation at 543 nm and emitted light collected
6 using a long-pass 560 nm filter. The pinhole was ~ 1 airy unit and the scanning frame was
7 512 \times 512 pixels. The cellular location of SPION was stained with the plasma membrane marker
8 CellMask (Invitrogen, USA), lysosome marker LysoTracker Green (Invitrogen, USA) and a
9 marker for cell nuclei, Hoechst 34580 (Invitrogen, USA). Image analysis was performed with
10 ZEN 2009 software (Zeiss, Germany). Co-localization was analyzed by a Pearson's efficiency
11 methods within ZEN 2009. The SPION-TRITC co-localization of lysosomes was calculated by
12 coefficient $c_{\text{SPION}} = \frac{\text{Pixel}_{\text{colocalized}}}{\text{Pixel}_{\text{total}}} \times 100$. Likewise, the LysoTracker-labeled lysosomes were
13 counted by coefficient $c_{\text{lysosome}} = \frac{\text{Pixel}_{\text{colocalized}}}{\text{Pixel}_{\text{total}}} \times 100$. The coefficient is reported as a percentage
14 from 0-100, with 0 meaning no co-localization and 100 meaning all pixel-pairs are co-localized.
15 Since TRITC labelled SPIONs were loaded into all the INS-1 cells after DMF treatment, we used
16 the fluorescence intensity of TRITC to indicate the amount of SPIONs in a cell after 3 times
17 washing. The total SPION loading efficiency was calculated by percentage of number of
18 fluorescence intensity of TRITC to the intensity of Hoechst 34580 which reflects cell number in
19 a field.

20 **Transmission electron microscopy (TEM) imaging.** The preparation of cells for TEM was
21 described previously.⁴² Briefly, INS-1 insulinoma tumor cells⁴³ were treated with DMF,
22 followed by fixation in 2.5% glutaraldehyde for 1h at 4 °C. The cells were then treated with 1%
23 osmium tetroxide, dehydrated, and embedded in AGAR100 (Oxford instruments Nordiska AB,
24 Stockholm) before being sliced in ultra-thin sections (70-90 nm). After slicing, the samples were
25
26
27
28
29
30
31
32
33
34
35
36
37
38
39
40
41
42
43
44

1
2
3 placed on Cu grids and contrasted with uranyl acetate and lead citrate. The TEM images were
4
5 obtained using a JEM 1230 electron microscope (Jeol-USA, Peabody, MA, USA).
6
7

8 **Human islet cell Immunostaining.** Human islets were provided by the EXODIAB Human
9
10 Tissue Lab and the Nordic Network of Clinical Islet Transplantation Programme
11
12 (www.nordicislets.org). The islet cells were separated in a Ca²⁺-free solution at 37 °C for 10 min.
13
14 and treated with DMF after 12 hour culture on the cover slips centered dish (MatTek, Germany).
15
16 Then the cells were fixed with 3% PFA-PIPES and 3% PFA-Na₂BO₄ for 5 min. and 10 min.,
17
18 respectively, followed by permeabilization with 0.1% Triton-X 100 for 30 min. and blocked with
19
20 5% normal donkey serum in PBS for 15 minutes. Guinea pig sourced antibody against insulin
21
22 (EuroProxima, Netherlands) was diluted in 5% block buffer and incubated overnight at 4 °C.
23
24 Immunoreactivity was done using fluorescently labeled secondary antibodies: cy2 anti-guinea
25
26 pig (1:400) and cy5 anti-mouse (1:400). The images of SPION-TRITC (EX: 543 nm), cy2-
27
28 labeled insulin (EX: 488 nm) and cy5-labeled LAMP1 (EX: 633 nm) visualized through three or
29
30 four channels by a confocal system (Zeiss, Germany). Lysosomal size (LAMP1 marked) was
31
32 calculated using the profile function of the ZEN 2009 software based on the shapes of the
33
34 fluorescence areas.
35
36
37
38
39

40
41 **Intracellular pH measurement.** INS-1 cells were seeded on the glass centered dish (MatTek,
42
43 Germany), loaded with SPION or SPION-LAMP1 and treated by DMF. Then the cells were
44
45 incubated with 1 μM acidic indicator, LysoSensor Green DND 189 (Invitrogen, USA) for 30 min.
46
47 in 37 °C. After incubation, the cells were washed out and the fluorescence images were acquired
48
49 by confocal microscopy. The average fluorescence intensity per cell was measured using the
50
51 ZEN 2009 software and further applied for quantitative analysis.
52
53
54
55
56
57
58
59
60

1
2
3 **Cell apoptosis detection.** FITC-Annexin V (51-65874X, BD, USA) and 7-AAD (51-68981E,
4 BD, USA) were used to assess early and late apoptosis of INS-1 cells. After DMF treatment, the
5 INS-1 cells were incubated with the dyes at 37 °C for 30 minutes. Images were acquired under
6 identical conditions (using the same settings for pinhole (1 airy unit), exposure time, gain and
7 scanning speed). Fluorescence intensity was analyzed by the ZEN 2009 software and early/late
8 stage apoptosis was quantified by percentage of number of Annexin V/7-AAD positive cells to
9 the number of Hoechst 34580 stained cells.

10
11 **Proliferation.** INS-1 cells were seeded on 24-well plates loaded with SPION or SPION-LAMP1
12 nanoparticles and treated by DMF once/day. Then the cell number was calculated by a plate
13 cytometer after 6 hours of DMF treatment. Cells were counted once per day for 5 days.

14
15 **Temperature measurements.** A dish with 100 nm SPIONs (10mg/ml) in water and a dish
16 without the SPIONs in water as a control, each containing a temperature sensor (Radial leaded
17 glass-encapsulated NTC thermistor, EPCOS Inc., Germany), were placed simultaneously on the
18 DMF device. The dishes were then subjected to the DMF field for 20 minutes at 20 Hz and the
19 temperature recorded in each dish.

20
21 **Statistical analysis.** The data was presented as average \pm standard error of the mean (S.E.M.).
22 Statistical comparison of paired-factors experiments was performed by Student's T-test and one-
23 way analysis of variance (ANOVA) and the Friedman tests were performed for multi-factor
24 experiments which have more than two group treatments in one experiment.
25
26
27
28
29
30
31
32
33
34
35
36
37
38
39
40
41
42
43
44
45
46
47
48
49
50
51
52
53
54
55
56
57
58
59
60

1
2
3 **Supporting Information Available:** Movie 1: Illustrates the rotational control of magnetic
4 micoparticles achieved with the DMF device. Movie 2: Illustrates the rotational control of
5 magnetic nanoparticles (300 nm diameter) achieved with the DMF device. Movie 3: Dynamic
6 confocal microscopy study of a single live cell illustrating injury to lysosomes *via* DMF and
7 LAMP1-SPIONs in real-time. This material is available free of charge *via* the Internet at
8 <http://pubs.acs.org>.
9
10
11
12
13
14
15
16
17
18
19
20
21
22
23
24
25
26
27
28
29
30
31
32
33
34
35
36
37
38
39
40
41
42
43
44
45
46
47
48
49
50
51
52
53
54
55
56
57
58
59
60

Acknowledgements

The authors would like to thank Dipl.-Ing. Ernst Stetter for front-line technology development necessary for the project, Britt-Marie Nilsson and Anna Veljanovska Ramsay for expert technical assistance. This study was funded in part by project grants from the Swedish Research Council (E.R. and L.E.); the NovoNordisk Foundation (E.R.); and Region Skåne/Lund University (ALF; E.R. and L.E.); NIH K08 CA16396 (M.F.K.); RSNA Research Resident and Scholar grants (RR0824, 2380) (M.F.K.); an MSKCC Center for Molecular Imaging and Nanotechnology Center grant (M.F.K.); an MSKCC Technology Development Grant (M.F.K.) and The Dana Foundation (M.F.K.). M.F.K. is a ‘Damon Runyon-Racleff Innovator’. The project has utilized infrastructure financed by the Linnaeus grant to Lund University Diabetes Center and the strategic research area in diabetes Exodiab. Human islets were obtained *via* the Exodiab Human Tissue Laboratory.

References

1. Gaster, R. S.; Hall, D. A.; Nielsen, C. H.; Osterfeld, S. J.; Yu, H.; Mach, K. E.; Wilson, R. J.; Murmann, B.; Liao, J. C.; Gambhir, S. S.; *et al.* Matrix-Insensitive Protein Assays Push the Limits of Biosensors in Medicine. *Nat. Med.* **2009**, *15*, 1327-1332.
2. Haun, J. B.; Yoon, T. J.; Lee, H.; Weissleder, R. Magnetic Nanoparticle Biosensors. *Wiley Interdiscip. Rev.: Nanomed. Nanobiotechnol.* **2010**, *2*, 291-304.
3. Haun, J. B.; Castro, C. M.; Wang, R.; Peterson, V. M.; Marinelli, B. S.; Lee, H.; Weissleder, R. Micro-Nmr for Rapid Molecular Analysis of Human Tumor Samples. *Sci. Transl. Med.* **2011**, *3*, 71ra16.
4. Haun, J. B.; Devaraj, N. K.; Marinelli, B. S.; Lee, H.; Weissleder, R. Probing Intracellular Biomarkers and Mediators of Cell Activation Using Nanosensors and Bioorthogonal Chemistry. *ACS Nano* **2011**, *5*, 3204-3213.
5. Kircher, M. F.; Gambhir, S. S.; Grimm, J. Noninvasive Cell-Tracking Methods. *Nat. Rev. Clin. Oncol.* **2011**, 677-688.
6. Kircher, M. F.; Mahmood, U.; King, R. S.; Weissleder, R.; Josephson, L. A Multimodal Nanoparticle for Preoperative Magnetic Resonance Imaging and Intraoperative Optical Brain Tumor Delineation. *Cancer Res.* **2003**, *63*, 8122-8125.
7. Kircher, M. F.; Willmann, J. K. Molecular Body Imaging: MR Imaging, CT, and US. Part II. Applications. *Radiology* **2012**, *264*, 349-368.
8. Kircher, M. F.; Willmann, J. K. Molecular Body Imaging: MR Imaging, CT, and US. Part I. Principles. *Radiology* **2012**, *263*, 633-643.
9. Grimm, J.; Kircher, M. F.; Weissleder, R. [Cell Tracking. Principles and Applications]. *Radiologe* **2007**, *47*, 25-33.
10. Kozissnik, B.; Bohorquez, A. C.; Dobson, J.; Rinaldi, C. Magnetic Fluid Hyperthermia: Advances, Challenges, and Opportunity. *Int. J. Hyperthermia* **2013**, *29*, 706-714.
11. Laurent, S.; Dutz, S.; Hafeli, U. O.; Mahmoudi, M. Magnetic Fluid Hyperthermia: Focus on Superparamagnetic Iron Oxide Nanoparticles. *Adv. Colloid Interface Sci.* **2011**, *166*, 8-23.
12. Guo, M.; Que, C.; Wang, C.; Liu, X.; Yan, H.; Liu, K. Multifunctional Superparamagnetic Nanocarriers with Folate-Mediated and Ph-Responsive Targeting Properties for Anticancer Drug Delivery. *Biomaterials* **2011**, *32*, 185-194.
13. Wahajuddin; Arora, S. Superparamagnetic Iron Oxide Nanoparticles: Magnetic Nanoplatfroms as Drug Carriers. *Int. J. Nanomed.* **2012**, *7*, 3445-3471.
14. Creixell, M.; Bohorquez, A. C.; Torres-Lugo, M.; Rinaldi, C. Egfr-Targeted Magnetic Nanoparticle Heaters Kill Cancer Cells without a Perceptible Temperature Rise. *ACS Nano* **2011**, *5*, 7124-7129.
15. Domenech, M.; Marrero-Berrios, I.; Torres-Lugo, M.; Rinaldi, C. Lysosomal Membrane Permeabilization by Targeted Magnetic Nanoparticles in Alternating Magnetic Fields. *ACS Nano* **2013**, *7*, 5091-5101.
16. Dobson, J. Remote Control of Cellular Behaviour with Magnetic Nanoparticles. *Nat. Nanotechnol.* **2008**, *3*, 139-143.
17. Corchero, J.; Villaverde, A. Biomedical Applications of Distally Controlled Magnetic Nanoparticles. *Trends Biotechnol.* **2009**, *27*, 468-476.
18. Kumar, C. S.; Mohammad, F. Magnetic Nanomaterials for Hyperthermia-Based Therapy and Controlled Drug Delivery. *Adv. Drug Delivery Rev.* **2011**, *63*, 789-808.

19. Wust, P.; Hildebrandt, B.; Sreenivasa, G.; Rau, B.; Gellermann, J.; Riess, H.; Felix, R.; Schlag, P. M. Hyperthermia in Combined Treatment of Cancer. *Lancet Oncol.* **2002**, *3*, 487-497.
20. Lee, J. H.; Jang, J. T.; Choi, J. S.; Moon, S. H.; Noh, S. H.; Kim, J. W.; Kim, J. G.; Kim, I. S.; Park, K. I.; Cheon, J. Exchange-Coupled Magnetic Nanoparticles for Efficient Heat Induction. *Nat. Nanotechnol.* **2011**, *6*, 418-422.
21. Ahmed, M.; Brace, C. L.; Lee, F. T., Jr.; Goldberg, S. N. Principles of and Advances in Percutaneous Ablation. *Radiology* **2011**, *258*, 351-369.
22. Gruttner, C.; Muller, K.; Teller, J.; Westphal, F.; Foreman, A.; Ivkov, R. Synthesis and Antibody Conjugation of Magnetic Nanoparticles with Improved Specific Power Absorption Rates for Alternating Magnetic Field Cancer Therapy. *J. Magn. Magn. Mater.* **2007**, *311*, 181-186.
23. El-Dakdouki, M. H.; Zhu, D. C.; El-Boubbou, K.; Kamat, M.; Chen, J. J.; Li, W.; Huang, X. F. Development of Multifunctional Hyaluronan-Coated Nanoparticles for Imaging and Drug Delivery to Cancer Cells. *Biomacromolecules* **2012**, *13*, 1144-1151.
24. Xu, H. F.; Dai, W.; Han, Y. H.; Hao, W.; Xiong, F.; Zhang, Y.; Cao, J. M. Differential Internalization of Superparamagnetic Iron Oxide Nanoparticles in Different Types of Cells. *J. Nanosci. Nanotechnol.* **2010**, *10*, 7406-7410.
25. Martin, A. L.; Hickey, J. L.; Ablack, A. L.; Lewis, J. D.; Luyt, L. G.; Gillies, E. R. Synthesis of Bombesin-Functionalized Iron Oxide Nanoparticles and Their Specific Uptake in Prostate Cancer Cells. *J. Nanopart. Res.* **2010**, *12*, 1599-1608.
26. Eto, K.; Yamashita, T.; Hirose, K.; Tsubamoto, Y.; Ainscow, E. K.; Rutter, G. A.; Kimura, S.; Noda, M.; Iino, M.; Kadowaki, T. Glucose Metabolism and Glutamate Analog Acutely Alkalinize Ph of Insulin Secretory Vesicles of Pancreatic Beta-Cells. *Am. J. Physiol. Endocrinol. Metab.* **2003**, *285*, E262-E271.
27. Cirman, T.; Oresic, K.; Mazovec, G. D.; Turk, V.; Reed, J. C.; Myers, R. M.; Salvesen, G. S.; Turk, B. Selective Disruption of Lysosomes in Hela Cells Triggers Apoptosis Mediated by Cleavage of Bid by Multiple Papain-Like Lysosomal Cathepsins. *J. Biol. Chem.* **2004**, *279*, 3578-3587.
28. Mannix, R. J.; Kumar, S.; Cassiola, F.; Montoya-Zavala, M.; Feinstein, E.; Prentiss, M.; Ingber, D. E. Nanomagnetic Actuation of Receptor-Mediated Signal Transduction. *Nat. Nanotechnol.* **2008**, *3*, 36-40.
29. Cho, M. H.; Lee, E. J.; Son, M.; Lee, J. H.; Yoo, D.; Kim, J. W.; Park, S. W.; Shin, J. S.; Cheon, J. A Magnetic Switch for the Control of Cell Death Signalling in *in Vitro* and *in Vivo* Systems. *Nat. Mater.* **2012**, *11*, 1038-1043.
30. Tseng, P.; Judy, J. W.; Di Carlo, D. Magnetic Nanoparticle-Mediated Massively Parallel Mechanical Modulation of Single-Cell Behavior. *Nat. Methods* **2012**, *9*, 1113-1119.
31. Ivkov, R.; DeNardo, S. J.; Daum, W.; Foreman, A. R.; Goldstein, R. C.; Nemkov, V. S.; DeNardo, G. L. Application of High Amplitude Alternating Magnetic Fields for Heat Induction of Nanoparticles Localized in Cancer. *Clin. Cancer Res.* **2005**, *11*, 7093s-7103s.
32. Huang, H.; Delikanli, S.; Zeng, H.; Ferkey, D. M.; Pralle, A. Remote Control of Ion Channels and Neurons through Magnetic-Field Heating of Nanoparticles. *Nat. Nanotechnol.* **2010**, *5*, 602-606.
33. Burckhardt, C. J.; Greber, U. F. Virus Movements on the Plasma Membrane Support Infection and Transmission between Cells. *PLoS Pathog.* **2009**, *5*, e1000621.
34. Tomasini, M. D.; Rinaldi, C.; Tomassone, M. S. Molecular Dynamics Simulations of Rupture in Lipid Bilayers. *Exp. Biol. Med. (Maywood)* **2010**, *235*, 181-188.

- 1
2
3 35. Ghosh, D.; Lee, Y.; Thomas, S.; Kohli, A. G.; Yun, D. S.; Belcher, A. M.; Kelly, K. A.
4 M13-Templated Magnetic Nanoparticles for Targeted *in Vivo* Imaging of Prostate Cancer. *Nat.*
5 *Nanotechnol.* **2012**, *7*, 677-682.
- 6
7 36. Gupta, A. K.; Gupta, M. Cytotoxicity Suppression and Cellular Uptake Enhancement of
8 Surface Modified Magnetic Nanoparticles. *Biomaterials* **2005**, *26*, 1565-1573.
- 9
10 37. Bogart, L. K.; Taylor, A.; Cesbron, Y.; Murray, P.; Levy, R. Photothermal Microscopy of
11 the Core of Dextran-Coated Iron Oxide Nanoparticles During Cell Uptake. *ACS Nano* **2012**, *6*,
12 5961-5971.
- 13 38. Schulze, K.; Koch, A.; Petri-Fink, A.; Steitz, B.; Kamau, S.; Hottiger, M.; Hilbe, M.;
14 Vaughan, L.; Hofmann, M.; Hofmann, H.; *et al.* Uptake and Biocompatibility of Functionalized
15 Poly(Vinylalcohol) Coated Superparamagnetic Maghemite Nanoparticles by Synoviocytes *in*
16 *Vitro*. *J. Nanosci. Nanotechnol.* **2006**, *6*, 2829-2840.
- 17
18 39. Amstad, E.; Kohlbrecher, J.; Muller, E.; Schweizer, T.; Textor, M.; Reimhult, E.
19 Triggered Release from Liposomes through Magnetic Actuation of Iron Oxide Nanoparticle
20 Containing Membranes. *Nano Lett.* **2011**, *11*, 1664-1670.
- 21
22 40. Daniel, W. A.; Wojcikowski, J. Lysosomal Trapping as an Important Mechanism
23 Involved in the Cellular Distribution of Perazine and in Pharmacokinetic Interaction with
24 Antidepressants. *Eur. Neuropsychopharmacol.* **1999**, *9*, 483-491.
- 25
26 41. Kornhuber, J.; Henkel, A. W.; Groemer, T. W.; Stadtler, S.; Welzel, O.; Tripal, P.; Rotter,
27 A.; Bleich, S.; Trapp, S. Lipophilic Cationic Drugs Increase the Permeability of Lysosomal
28 Membranes in a Cell Culture System. *J. Cell. Physiol.* **2010**, *224*, 152-164.
- 29
30 42. Vikman, J.; Jimenez-Feltstrom, J.; Nyman, P.; Thelin, J.; Eliasson, L. Insulin Secretion Is
31 Highly Sensitive to Desorption of Plasma Membrane Cholesterol. *FASEB J.* **2009**, *23*, 58-67.
- 32
33 43. Asfari, M.; Janjic, D.; Meda, P.; Li, G.; Halban, P. A.; Wollheim, C. B. Establishment of
34 2-Mercaptoethanol-Dependent Differentiated Insulin-Secreting Cell Lines. *Endocrinology* **1992**,
35 130, 167-178.
- 36
37
38
39
40
41
42
43
44
45
46
47
48
49
50
51
52
53
54
55
56
57
58
59
60